Computing Reconstruction Kernels for circular 3D Cone Beam Tomography

Alfred K Louis, Thomas Weber and David Theis

***Abstract*—In this paper we present techniques for deriving inversion algorithms in 3D computer tomography. To this end we introduce the mathematical model and apply a general strategy, the so-called approximate inverse, for deriving both exact and numerical inversion formulas. Using further approximations, we derive a 2D shift-invariant filter for circular-orbit cone-beam imaging. Results from real data are presented.**

***Index Terms*—X-ray tomography, cone-beam CT, inverse problems, mollifier, reconstruction kernel**

I. Introduction

The circular scanning geometry presently is the most widely used scanning modality in non-destructive 3D X-ray CT. The well known Feldkamp algorithm is still often used, despite its drawbacks in the case of large cone angles. In this paper we derive fast inversion algorithms, using a strategy which can be applied to almost arbitrary scanning geometries. It is based on the *approximate inverse*, where reconstruction kernels are pre-computed independently of the data.

In the first section we summarize results from the approximate inverse, then we describe the relation between X-ray and Radon transform, the *formula of Grangeat*. We apply both ingredients to derive firstly an exact inversion formula. This is then used to calculate, based on user prescribed mollifiers, the reconstruction kernel with given smoothing properties for damping the influence of the unavoidable measurement errors. In the derivation of the inversion algorithm, the formula of Grangeat is used. The algorithm itself is completely different from Grangeat's algorithm, the numerically critical operations are not performed on the detector, but on the mollifier. Also, there is no rebinning of the data needed. In the following we derive analytical formulas for the evaluation of these kernels for the circular scanning geometry.

In the last section we present images of the reconstruction kernel and of reconstructions from real data.

II. Approximate Inverse

The integral operators appearing in most tomographic problems are compact operators acting on suitable Hilbert spaces with infinite dimensional ranges. Hence, their inverse operators are not continuous, which means that data errors are amplified in the solution. So we concentrate on finding approximate inversion formulas, that allow for a compromise between best possible accuracy and necessary damping of data errors appearing in any real measurement.

Department of Mathematics, Saarland University, 66041 Saarbrücken, Germany. Corresponding author: Alfred K Louis, E-mail: louis@num.uni-sb.de.

The research of the authors has been supported by the Deutsche Forschungsgemeinschaft under grant LO 310/8-1.

For approximating the solution of

$$Af = g,$$

with an operator $A : X \to Y$ acting on suitable Hilbert spaces, we apply the method of approximate inverse, see [1]. The basic idea is as follows: we choose a *mollifier* $e_\gamma(x, y)$, which, for a fixed reconstruction point x, is a function of the variable y and as such approximates the delta distribution for the point x. The parameter γ acts as regularization parameter, i.e. $e_\gamma(x, y) \to \delta_x(y)$ for $\gamma \to 0$.

For a fixed reconstruction point x, we solve the auxiliary problem

$$A^*\psi_\gamma(x, \cdot) = e_\gamma(x, \cdot), \tag{1}$$

where $e_\gamma(x, \cdot)$ is our chosen approximation of $\delta_x(\cdot)$ and A^* denotes the adjoint of A. The searched-for function $\psi_\gamma(x, \cdot)$ is the *reconstruction kernel*. For the approximate solution f_γ we then get

$$\begin{aligned} f_\gamma(x) &= \left\langle f, e_\gamma(x, .)\right\rangle_X = \left\langle f, A^*\psi_\gamma(x, \cdot)\right\rangle_X \\ &= \left\langle Af, \psi_\gamma(x, \cdot)\right\rangle_Y = \left\langle g, \psi_\gamma(x, \cdot)\right\rangle_Y \\ &=: S_\gamma g(x), \end{aligned}$$

where the operator S_γ is called the *approximate inverse*.

At first glance, this does not look like an improvement, since we have to solve an equation for the adjoint of our original operator A. But this problem can be solved independently of the data, i.e. well in advance. Furthermore, invariances and symmetries of the operator A^* can directly be transformed into corresponding properties of S_γ, see [1] and section V-A.

This method is presented in [2] as a general regularization scheme to solve inverse problems. Generalizations are also given. The application to vector fields was derived by Schuster [3]. If the auxiliary problem is not solvable then its minimum norm solution leads to the minimum norm solution of the original problem.

III. Inversion Formula for the 3D Cone Beam Transform

In the following we consider the X-ray reconstruction problem in three dimensions when the data are measured by firing an X-ray tube emitting rays to a 2D detector. The movement of the combination source – detector determines the different scanning geometries. In many real-world applications the source is moved on a circle around the object. From a mathematical point of view this has the disadvantage that the data are incomplete, the condition of Tuy-Kirillov is not fulfilled. We base our considerations on the assumption that this condition is satisfied, the reconstruction from real data nevertheless is then from the above described circular scanning geometry, because other data are not available to us so far.

A first theoretical presentation of the reconstruction kernel was given by Finch [4]. The use of invariance properties was a first step towards practical implementations, see [5]. See also the often used algorithm of Feldkamp et al. [6] and the contribution of Defrise and Clack [7]. A unified approach to those papers is contained in [8]. The approach of Katsevich [9] differs from ours in that he avoids the Crofton symbol by restricting the back projection to a range dependent on the reconstruction point x.

A. *Mathematical model*

We denote with $a \in \Gamma$ the source position, where $\Gamma \subset \mathbb{R}^3$ is a curve, and $\theta \in S^2$ is the direction of the ray. Then the cone-beam transform of a function $f \in L_2(\mathbb{R})$ is defined as

$$\mathbf{D}f(a,\theta) = \int_0^\infty f(a+t\theta)\,dt. \tag{2}$$

The adjoint operator as mapping from $L_2(\mathbb{R}^3) \to L_2(\Gamma \times S^2)$ is given as

$$\mathbf{D}^* g(x) = \int_\Gamma \|x-a\|^{-2}\; g\left(a, \frac{x-a}{\|x-a\|}\right) da. \tag{3}$$

Most attempts to find inversion formulae are based on the *Formula of Grangeat*, first published in Grangeat's PhD thesis [10], see also [11]:

$$\frac{\partial}{\partial s}\mathbf{R}f(\omega,s)\Big|_{s=\langle a,\omega\rangle} = -\int_{S^2} \mathbf{D}f(a,\theta)\delta'(\langle\theta,\omega\rangle)\,d\theta. \tag{4}$$

Our starting point is now the inversion formula for the 3D Radon transform

$$f(x) = -\frac{1}{8\pi^2}\int_{S^2} \frac{\partial^2}{\partial s^2}\mathbf{R}f(\omega,s)\Big|_{s=\langle x,\omega\rangle} d\omega, \tag{5}$$

that we rewrite as

$$f(x) = \frac{1}{8\pi^2}\int_{S^2}\int_{\mathbb{R}} \frac{\partial}{\partial s}\mathbf{R}f(\omega,s)\delta'(s-\langle x,\omega\rangle)\,ds\,d\omega. \tag{6}$$

We assume in the following that the TuyKirillov condition is fulfilled. Then we can change the variables as follows: By $n(\omega,s)$ we denote the Crofton symbol, i.e. the number of source points $a \in \Gamma$ such that $\langle a,\omega\rangle = s$:

$$n(\omega,s) = \#\{a \in \Gamma : \langle a,\omega\rangle = s\}.$$

Setting $m = 1/n$, we get

$$\begin{aligned} f(x) &= \frac{1}{8\pi^2}\int_{S^2}\int_\Gamma (\mathbf{R}f)'(\omega,\langle a,\omega\rangle)\,\delta'(\langle a-x,\omega\rangle) \\ &\quad\times |\langle \dot a,\omega\rangle|\, m(\omega,\langle a,\omega\rangle)\,da\,d\omega \\ &= -\frac{1}{8\pi^2}\int_{S^2}\int_\Gamma\int_{S^2} \mathbf{D}f(a,\theta)\,\delta'(\langle\theta,\omega\rangle)\,d\theta \\ &\quad\times \delta'(\langle a-x,\omega\rangle)\,|\langle\dot a,\omega\rangle|\, m(\omega,\langle a,\omega\rangle)\,da\,d\omega \\ &= +\frac{1}{8\pi^2}\int_\Gamma \frac{1}{\|x-a\|^2}\int_{S^2}\int_{S^2}\mathbf{D}f(a,\theta)\,\delta'(\langle\theta,\omega\rangle)\,d\theta \\ &\quad\times \delta'(\left\langle \frac{x-a}{\|x-a\|},\omega\right\rangle)\; |\langle\dot a,\omega\rangle|\; m(\omega,\langle a,\omega\rangle)\,da\,d\omega \end{aligned}$$

where we used that δ' is homogeneous of degree -2 and that $\delta'(-s) = -\delta'(s)$. We now introduce the operator

$$T_1 g(\omega) = \int_{S^2} g(\theta)\,\delta'(\langle\theta,\omega\rangle)\,d\theta, \tag{7}$$

acting on the second variable of a function $g(a,\omega)$ as

$$T_{1,a}g(\omega) = T_1 g(a,\omega),$$

and the multiplication operator

$$M_\Gamma\, h(a,\theta) = |\langle\dot a,\omega\rangle|\;\, m(\omega,\langle a,\omega\rangle)\,h(\omega) \tag{8}$$

and state the following result, see also [12].

Theorem 3.1: Let the condition of Tuy-Kirillov be fulfilled. Then the inversion formula for the cone beam transform is given as

$$f = \frac{1}{8\pi^2}\mathbf{D}^* T_1 M_\Gamma T_1 \mathbf{D} f$$

with the adjoint operator $\mathbf{D}^*$ of the cone beam transform and T_1 and M_Γ as defined above.

□

Note that both $\mathbf{D}^*$ and M_Γ depend on the scanning curve Γ, whereas T_1 only depends on the specific point a of the scanning curve.

The above theorem allows for computing reconstruction kernels. To this end we have to solve the equation

$$\mathbf{D}^*\psi_\gamma = e_\gamma,$$

in order to write the solution of $\mathbf{D}f = g$ as

$$f(x) = \left\langle g, \psi_\gamma(x,\cdot)\right\rangle_Y.$$

In the case of exact inversion, e_γ is the delta distribution, in the case of an approximate inversion formula, it is an approximation of this distribution. From the above we see that

$$\mathbf{D}^{-1} = \frac{1}{8\pi^2}\mathbf{D}^* T_1 M_\Gamma T_1$$

and we can write

$$\mathbf{D}^*\psi_\gamma = e_\gamma = \frac{1}{8\pi^2}\mathbf{D}^* T_1 M_\Gamma T_1 \mathbf{D} e_\gamma,$$

hence

$$\psi_\gamma = \frac{1}{8\pi^2} T_1 M_\Gamma T_1 \mathbf{D} e_\gamma. \tag{9}$$

IV. Computing the reconstruction kernel

In the following, we will use (9) to derive an analytic formula for the reconstruction kernel in 3D. We use the gaussian

$$e_\gamma(x,y) = (2\pi)^{-3/2}\frac{1}{\gamma^3}e^{-\frac{\|x-y\|^2}{2\gamma^2}} \tag{10}$$

as mollifier (which we write as $e_x(y)$) and get

$$T_1 D e_\gamma(a,\omega,x) = \frac{(2\pi)^{-1/2}}{\gamma^3}\; e^{-\frac{1}{2\gamma^2}\langle a-x,\omega\rangle^2}\;\langle a-x,\omega\rangle\,. \tag{11}$$

Proof: Following [13, p. 69], we have

$$\int_{S^2}[Df](a,\theta)\delta'(\langle\theta,\omega\rangle)\,d\theta = -\int_{\omega^\perp}\langle[\nabla f](\langle a,\omega\rangle\,\omega + y),\omega\rangle\; dy.$$

For the gaussian, this means

$$\begin{aligned}
[T_1 De_x](a,\omega) &= -\int_{\omega^\perp + a} \left\langle [\nabla_y e_x](y), \omega \right\rangle \, dy \\
&= \frac{1}{\gamma^2} \left\langle \int_{\omega^\perp + a} e(\|y-x\|)(y-x)\, dy, \omega \right\rangle \\
&= \frac{(2\pi)^{-3/2}}{\gamma^5} \int_{\omega^\perp} \exp(-\frac{1}{2\gamma^2}\|y+z\|^2)(y+z)\, dy.
\end{aligned}$$

We introduce a rotated coordinate system, such that ω is one of the directions. As we only integrate over $\omega^\perp$, the integral reduces to an integration over $\mathbb{R}^2$ and yields the mentioned result. ■

For the multiplication operator M_Γ, we need the inverse of the Crofton symbol, m. For the specific case of a circular scanning geometry, we set $n = 2$ and hence $m = 1/2$. Applying the operator T_1 to the function in (11) yields the following result.

Theorem 4.1: Let the scanning curve Γ be a circle with radius R and the density function f fulfils $\operatorname{supp} f \subset r \cdot S^2, r < R$. If the direction vector $\theta \in S^2$ does not lie parallel to the vector $x - a$, the reconstruction kernel ψ can be written as

$$\begin{aligned}
\psi_\gamma(a,\theta,x) = -\frac{C}{2\pi}\Big[\frac{p_3}{p_4}\Big\{ \langle \dot{a}, \theta\rangle - 2\alpha \langle a - x, \theta\rangle p_3 \Big\} \\
\times \int_0^1 e^{p_1[p_2 t^2 - 1]}\, dt + p_4 \langle a - x, \theta\rangle e^{p_1[p_2 - 1]}\Big],
\end{aligned} \tag{12}$$

where

$$\begin{aligned}
\alpha &:= \frac{1}{2\gamma^2}, \qquad C := (2\pi)^{-3/2}\frac{1}{\gamma^3} \\
p_1 &:= \alpha \, \|a - x - \langle a - x, \theta\rangle \theta\|^2 \\
p_2 &:= \frac{\langle a - x - \langle a - x, \theta\rangle \theta, \dot{a} - \langle \dot{a}, \theta\rangle \theta\rangle^2}{\|\dot{a} - \langle \dot{a}, \theta\rangle \theta\|^2 \, \|a - x - \langle a - x, \theta\rangle \theta\|^2} \\
p_3 &:= \langle a - x - \langle a - x, \theta\rangle \theta, \dot{a} - \langle \dot{a}, \theta\rangle \theta\rangle \\
p_4 &:= \|\dot{a} - \langle \dot{a}, \theta\rangle \theta\| \, .
\end{aligned}$$

If θ lies parallel to $x - a$, then the kernel can be calculated as

$$\psi_\gamma(a,\theta,x) = -\frac{C}{2\pi}\|\dot{a} - \langle \dot{a}, \theta\rangle \theta\|^2 \langle a - x, \theta\rangle \, . \tag{13}$$

□

Theorem 4.1 provides a means for fast computations of reconstruction kernels, eliminating the need for pre-computed kernels. Figure 1 shows the shape of such a kernel. The calculation of this kernel took approximately 6.6 seconds on a x86 desktop system with a 3 GHz CPU, the discrete kernel has 513^2 elements.

Remark 4.2: The circle used in theorem 4.1 does not fulfil the Tuy-Kirillov condition, hence the theorem only provides an approximative solution. With respect to the 3D Radon transform, this leads to hollow projections. In the 2D case, uniqueness is preserved, in 3D this is subject of future research. With respect to the long object problem, one additionally faces truncated projections which means that other scanning geometries, like helices are to be preferred.

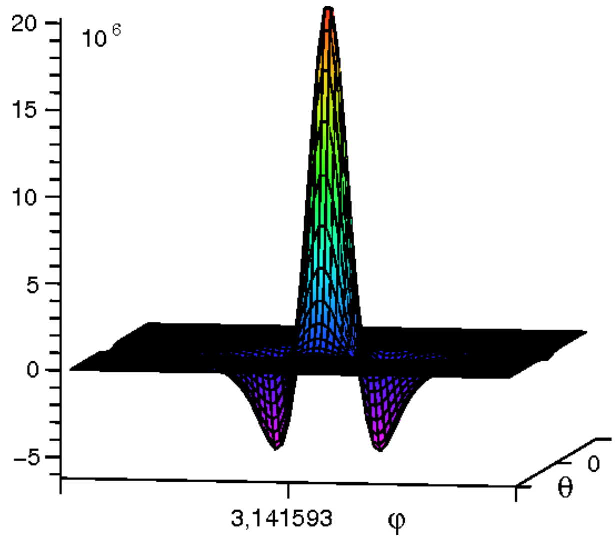

Fig. 1. 3D Plot of a kernel for 513x513 detector points, with $\gamma = 0.00165$.

V. Implementation

A. Invariances

As mentioned, using the approximate inverse (AI), invariances of the operator can be used to shorten the calculation of the reconstruction kernel. Using our explicit formula for ψ, we easily see the following:

1) The reconstruction kernel depends only via $a - x$ on x, i.e. only the relative vector between a and x is important.
2) For the point $x = 0$, we have

$$\psi_\gamma(Va, \theta, x = 0) = \psi_\gamma(a, V^{\mathrm{T}}\theta, x = 0)$$

for every rotation matrix V.

The second invariance is only true for the point $x = 0$. A first step towards a fast and easy computation of a reconstruction kernel was taken by Dietz in his PhD thesis, see [13]. But whereas he used a reconstruction kernel for the 3D Radon transform and subsequently calculated a numerical kernel for the ray transform, we use equation (9) to derive an analytical formula for the reconstruction for the X-ray transform. Using this formula, we can overcome the need for a pre-computed kernel, which gives us more flexibility.

For the approximate invariance, we define ${U_x}^{\mathrm{T}}$ to be the rotation matrix that rotates $\frac{a-x}{\|a-x\|}$ onto a/R, i.e.

$${U_x}^{\mathrm{T}}\frac{a-x}{\|a-x\|} = \frac{a}{R}.$$

For real world measurement setups, U_x will be so "close" to the identity matrix that we can then assume $U_x\dot{a} = \dot{a}$. The reason for that is that the radius of the sphere in which we reconstruct is (much) smaller than the radius of the source curve. Then, instead of calculating the reconstruction kernel for different values of x, we calculate it only for $x = 0$ and scale it by a factor of $\frac{R^2}{\|a-x\|^2}$, see [13]

$$\psi(a,\theta,x) \approx \frac{R^2}{\|a-x\|}\psi(a, {U_x}^{\mathrm{T}}\theta, x = 0).$$

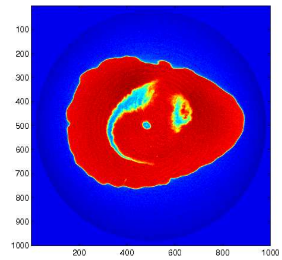

(a) Reconstruction at height $z = -0.22$.

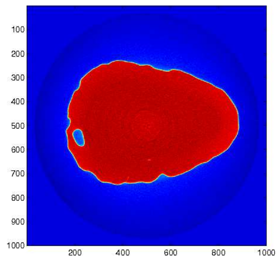

(b) Reconstruction at height $z = -0.28$.

Measurement parameters	
Detector array	1024×1024
Projections	800
Source – Detector	~ 126 cm
Source – Object	~ 5.1 cm
Reconstruction parameters	
Reconstruction grid	1000×1000
γ	0.00165 cm

(c) Parameters

(d) Original bust

Fig. 2. Reconstruction of a bust

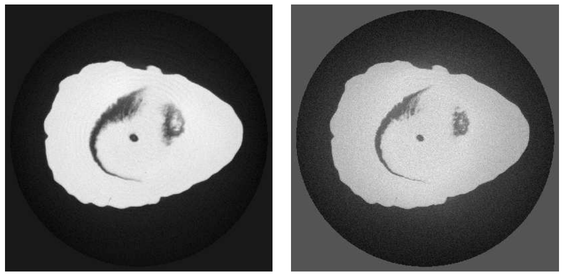

(a) Approximate Inverse (b) Feldkamp with RamLak filter

Fig. 3. Comparing the reconstruction with the Feldkamp algorithm. The black circle marks the reconstruction area. Parameters are the same as in figure 2.

Tying these invariances together, we see that we only need to compute the kernel once for one value of a and the different ray directions θ. The different reconstruction points x are taken into account by the simple scaling factor above.

B. Computational complexity

With the invariances detailed in subsection V-A we can implement the approximate inverse with the very same complexity as the FDK algorithm:

1) Generate the filter matrix and calculate its Fourier transform (once!).
2) For each source point a
   a) Calculate the Fourier transform of the data matrix (that is, the matrix with the measured data).
   b) Multiply both matrices element-wise and calculate the inverse Fourier transform of the resulting matrix.
3) Use these matrices for the back projection.

The only different part is the computation of the kernel 3D-matrix. As mentioned after theorem 4.1, the kernel computation takes only a few seconds, so this part is negligible. Thus, the two algorithms are on par with respect to their computational requirements.

In the following section, we present reconstructions from real data, kindly provided by Fraunhofer IzfP, Saarbrücken.

VI. Reconstructions from real data

In figure 2, we reconstructed a bust, showing Joseph von Fraunhofer. One can clearly see that there are air locks inside the bust. Also, the algorithm gives a smooth reconstruction of the interior area.

We compared our algorithm with the well-known Feldkamp-algorithm, using a Shepp filter. The results in figure 3 show that especially near the boundary of the reconstruction area, our algorithm gives a better impression of the rather homogeneous material.

In figure 5, we reconstructed an artificial real test object, consisting of layers of aluminium and adhesive. This test object is used to test algorithms for their resolution in the z-direction.

For the Shepp filter, one needs the essential bandwidth Ω of the function f in order to choose the step size between different detector points according to the Nyquist rate, see [14]. Obviously, we do not know the function's essential bandwidth and (even if we knew it) we cannot change the physical detector layout. So we assume the function to have the bandwidth $\Omega_{ess} = \frac{\pi}{h}$, where h is the step size on the detector.

As can be seen in figure 4(a), this leads to a very poor reconstruction. In figures 4(b) and 4(c), we therefore used a Shepp filter with a bandwidth of $\Omega = \frac{\pi}{5h}$ and $\Omega = \frac{\pi}{10h}$, respectively. This yields results with an acceptable noise level.

A reconstruction with our proposed method is shown in figure 5. There's no further smoothing necessary, the regularization parameter γ is taking care of that for us.

We can clearly distinguish the disruptions over the whole object, which shows that – despite the circular scanning curve – the reconstruction in z-direction is very good. The vertical artefact right from the middle is known to come from the physical detector setup used for the measurement.

Choosing a smaller bandwidth as explained above for the Shepp filter yields a worse resolution, which can be seen in the magnification of the lower right corner in figure 6(b). This shows that the Feldkamp reconstruction with the smallest bandwidth looks good in the large picture, but it's actually blurry. The Feldkamp reconstruction with a bandwidth of $\Omega_{ess}/5$ conserves the edges much better. The approximate inverse gives a comparable result with less noise.

In order to better understand the quality issues, we have plotted cross sections of the reconstructions in figures 7 and 8. The intersections are taken at the white lines shown in figure 4(a).

For the horizontal intersection in figure 7, we see that at the end of the aluminium block (around pixel 300), the AI reconstruction goes down almost vertically, indicating the sharp edge of the metal block. The FDK reconstruction has a lesser slope, leading to a blurry edge. Additionally, there's

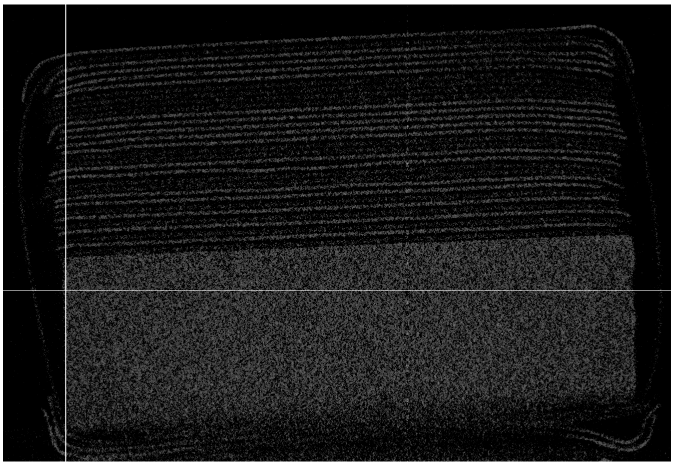

(a) Bandwidth Ω_{ess} according to the Nyquist rate.

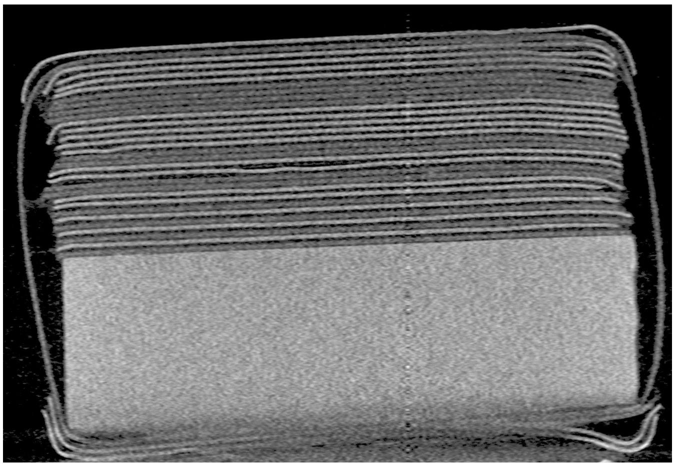

(b) Bandwidth $\Omega_{ess}/5$.

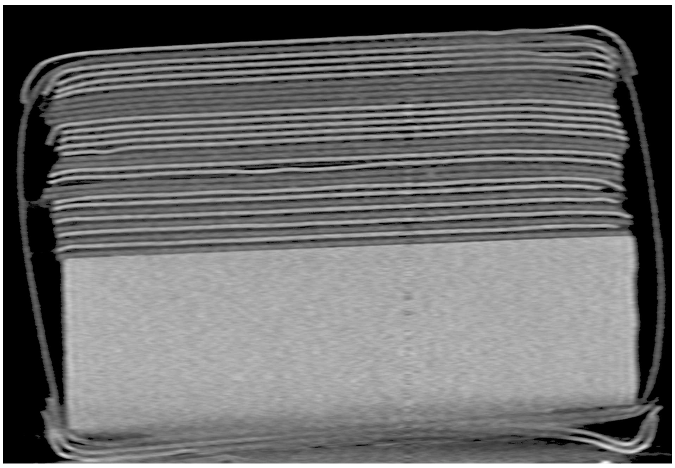

(c) Bandwidth $\Omega_{ess}/10$.

Fig. 4. Reconstruction of an artificial test object, consisting of layers of aluminium and adhesive. The images show a reconstruction at $x = 0.0$ with the Feldkamp algorithm using a Shepp filter with different bandwidths. The default bandwidth according to the Nyquist rate leads to a grainy resolution. The horizontal and vertical lines in the first image indicate where we draw the cross section in figure 7 and figure 8, respectively.

Measurement parameters	
Detector array	1024×1024
Projections	400
Source – Detector	~ 126 cm
Source – Object	~ 2.9 cm
Reconstruction parameters	
Reconstruction grid	3000×3000
γ	0.00062 cm

(a) Parameters

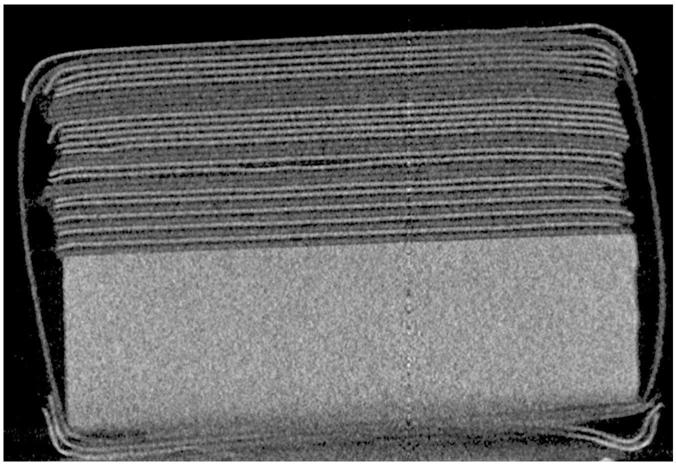

(b) Approximate inverse.

Fig. 5. Reconstruction of the the aluminium layers with our proposed method. Noise level is lower than even with the best of the three Feldkamp reconstructions, whereas resolution is at least at par. The parameters for the reconstruction can be found in table 5(a)

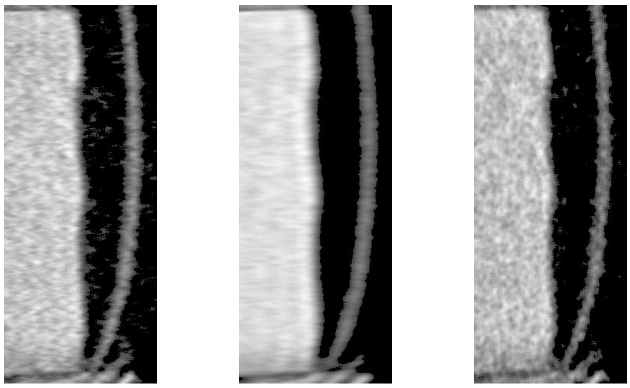

(a) Bandwidth $\Omega_{ess}/5$. (b) Bandwidth $\Omega_{ess}/10$. (c) $\gamma = 0.00062cm$.

Fig. 6. Magnification of the lower right corner. The left and middle picture show the FDK algorithm with the mentioned bandwidth, the right picture shows the reconstruction with the AI. The resolution of the Feldkamp reconstruction becomes too bad if we choose the bandwidth too low.

some noise at the edge (around pixel 330), again showing that the FDK reconstruction has a lower resolution. The outer foil (starting at about pixel 370) also is smaller in the AI reconstruction.

With respect to the vertical intersection in figure 8, we see that at around pixel 80, the AI reconstruction separates the two foils clearly, whereas the FDK reconstruction has an artefact there. Generally, the AI reconstuction tends to show the sharp edges of the different layers better.

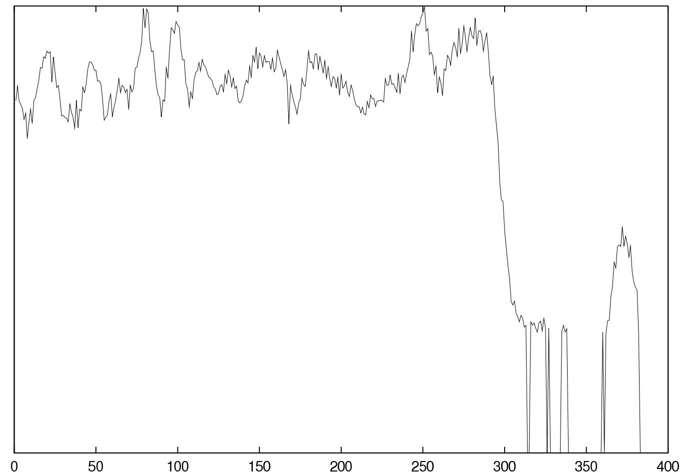

(a) Feldkamp

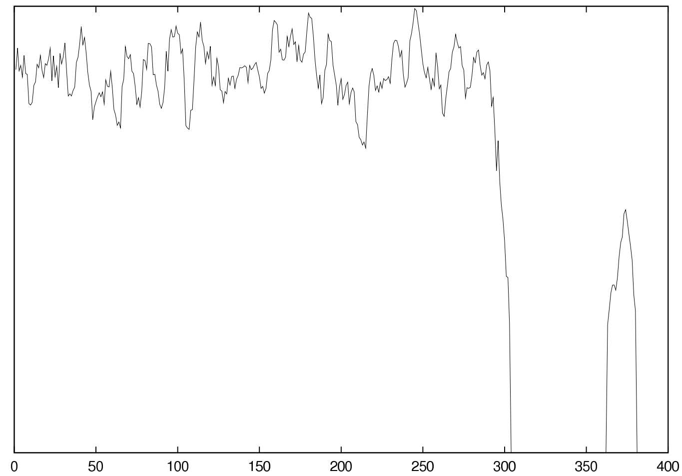

(b) Approximate Inverse

Fig. 7. Horizontal cross section of the reconstructions with a bandwidth of $\Omega_{ess}/5$ and a value of $\gamma = 0.00062cm$, respectively. The plot shows only the right part of the intersection for clarity.

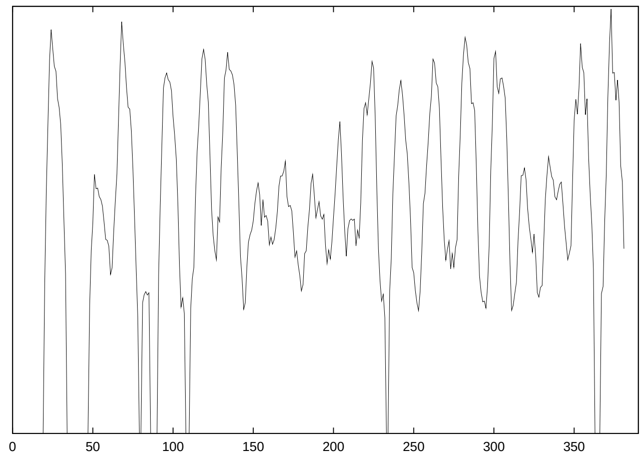

(a) Feldkamp

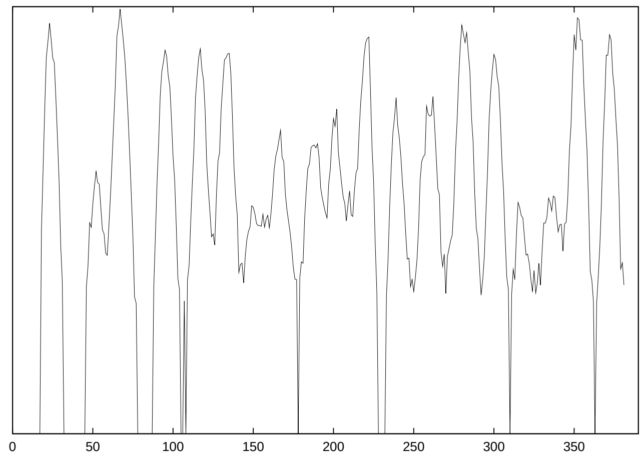

(b) Approximate Inverse

Fig. 8. Vertical section of the reconstructions with a bandwidth of $\Omega_{ess}/5$ and a value of $\gamma = 0.00062cm$, respectively. The plot is starting at the top of the image (leaving out most of the background) and shows only a small part of the intersection for clarity.

VII. Conclusion

We have presented an exact inversion formula and derived a suitable numerical inversion formula from it for the circular scanning geometry. The numerical implementation is fast enough to no longer rely on a pre-computed kernel. Instead, the kernel can be computed as part of the measurement. As such, our method has the same numerical complexity as the Feldkamp algorithm. However, the approximate inverse has both a better resolution and a lower noise level.

In the future, we want to apply this approach also to helical scanning geometries, since scanning times become more and more important in all real applications, e.g. in non-destructive testing and especially in medical diagnostics.

References

[1] A. K. Louis, “Approximate inverse for linear and some nonlinear problems,” *Inverse Problems*, vol. 12, no. 2, pp. 175–190, 1996. [Online]. Available: http://stacks.iop.org/0266-5611/12/175

[2] ——, “A unified approach to regularization methods for linear ill-posed problems,” *Inverse Problems*, vol. 15, no. 2, pp. 489–498, 1999. [Online]. Available: http://stacks.iop.org/0266-5611/15/489

[3] T. Schuster, “The 3d doppler transform: elementary properties and computation of reconstruction kernels,” *Inverse Problems*, vol. 16, no. 3, pp. 701–722, 2000. [Online]. Available: http://stacks.iop.org/0266-5611/16/701

[4] D. V. Finch, “Approximate reconstruction formulae for the cone beam transform, I.” 1987, unpublished. [Online]. Available: http://www.math.oregonstate.edu/~finch/papers/postcone.pdf

[5] A. K. Louis, “Filter design in three-dimensional cone beam tomography: circular scanning geometry,” *Inverse Problems*, vol. 19, no. 6, pp. S31–S40, 2003. [Online]. Available: http://stacks.iop.org/0266-5611/19/S31

[6] L. Feldkamp, L. Davis, and J.W.Kress, “Practical cone beam algorithm,” *Journal of the Optical Society of America A*, vol. 1, no. 6, pp. 612–619, 1984. [Online]. Available: http://www.opticsinfobase.org/abstract.cfm?URI=josaa-1-6-612

[7] M. Defrise and R. Clack, “A cone-beam reconstruction algorithm using shift-invariant filtering and cone-beam backprojection,” *IEEE Transactions on Medical Imaging*, vol. 13, no. 1, pp. 186–195, 1994. [Online]. Available: http://ieeexplore.ieee.org/xpl/freeabs_all.jsp?isnumber=6838&arnumber=276157

[8] S. Zhao, H. Yu, and G. Wang, “A unified framework for exact cone-beam reconstruction formulas,” *Medical Physics*, vol. 32, no. 6, pp. 1712–1721, 2005. [Online]. Available: http://link.aip.org/link/?MPH/32/1712/1

[9] A. Katsevich, “Analysis of an exact inversion algorithm for spiral cone-beam ct,” *Physics in Medicine and Biology*, vol. 47, no. 15, pp. 2583–2597, 2002. [Online]. Available: http://stacks.iop.org/0031-9155/47/2583

[10] P. Grangeat, “Analyse d’un système d’imagerie 3d par reconstruction à partir de radiographies x en géométrie conique,” Ph.D. dissertation, Ecole Nationale Supérieure des Télécommunications, 1987.

[11] ——, “Mathematical framework of cone beam 3D reconstruction via the first derivative of the Radon transform,” in *Mathematical Methods in Tomography*, ser. Lecture Notes in Mathematics, Gabor T. Herman and Alfred K. Louis and Frank Natterer, Ed. New York: Springer-Verlag, 1991, pp. 66–97, proceedings of a Conference held in Oberwolfach, Germany, 5-11 June, 1990.

[12] A. K. Louis, “Development of algorithms in computerized tomography,” in *The Radon Transform, Inverse Problems, and Tomography (Proceedings of Symposia in Applied Mathematics)*, ser. Proceedings of Symposia in Applied Mathematics, G. Olafsson and E. T. Quinto, Eds., vol. 63. Boston, MA, USA: AMS, 2006, pp. 25–42.

[13] R. Dietz, “Die approximative inverse als rekonstruktionsmethode in der röntgen-computertomographie,” Ph.D. dissertation, Mathematisch-Naturwissenschaftliche Fakultät der Universität des Saarlandes, 1999.

[14] F. Natterer and F. Wuebbeling, *Mathematical Methods in Image Reconstruction*. Philadelphia: SIAM, 2001.